JOURNAL OF GEOPHYSICAL RESEARCH, VOL. 115, B03101, doi:10.1029/2009JB006390, 2010

Compatibility of induction methods for mantle soundings

J. Vozar[1,2] and V. Y. Semenov[3]

Received 16 February 2009; revised 17 July 2009; accepted 30 September 2009; published 17 March 2010.

[1] Formulations that form the basis of experimental impedances in induction soundings result from the impedance boundary conditions or from the simplified theoretical models. The formulations are essentially different for the magnetotelluric and magnetovariation sounding methods. In order to increase reliability of mantle investigations, studies of the mantle's electrical properties are often carried out by the joint inversion of impedances obtained by both sounding methods. A forward modeling approach is used to verify the accuracy of merging the long-period impedances obtained by the magnetotelluric and magnetovariation methods. The spherical modeling of the responses above 2-D and 3-D mantle inhomogeneities has shown that the different induction methods can give mutually inconsistent results and the combination of their responses can be problematic in practice. For this reason much attention is given to the generalized horizontal spatial gradient sounding method which results in impedance functions that in space and frequency domains closely resemble the magnetotelluric impedances. In this study some interesting properties of the induction arrows above a spherical inhomogeneity, excited by an inhomogeneous external field, are estimated for long periods. A final comprehensive model, assuming a shell of realistic conductance at the Earth's surface, is evidence that the generalized horizontal spatial gradient method is promising for the study of mantle inhomogeneities and can be reliably used in combination with the magnetotelluric method in a specific way.

Citation: Vozar, J., and V. Y. Semenov (2010), Compatibility of induction methods for mantle soundings, *J. Geophys. Res.*, *115*, B03101, doi:10.1029/2009JB006390.

1. Introduction

[2] Induction soundings of the Earth's mantle and their interpretations are based on response functions obtained by both the magnetotelluric (MT) and the magnetovariation (MV) methods. The latter soundings have been previously represented by both the horizontal spatial gradient (HSG) sounding method [*Berdichevsky et al.*, 1969; *Schmucker*, 1970; *Kuckes*, 1973] and the geomagnetic depth sounding (GDS) method [*Banks*, 1969]. The GDS method has often been applied to real data, for example, by *Roberts* [1984], *Schultz and Larsen* [1987], *Olsen* [1998], and O. Praus et al. (Electrical conductivity at midmantle depths estimated from the data of Sq and long period geomagnetic variations, submitted to *Studia Geophysica et Geodaetica,* 2009), while the HSG method has been used rather rarely to date [*Lilley et al.*, 1981; *Jones*, 1982; *Hermance and Wang*, 1992; *Logvinov*, 2002]. Recently the "generalized" HSG method was introduced by *Shuman and Kulik* [2002] and by *Schmucker* [2003].

[3] The MT and MV experimental impedances determined from the relationships between the observed magnetic and electric fields are entirely different: e.g., tensor and local for MT and scalar and regional for MV (scattering for HSG [*Kuckes et al.*, 1985]) methods. Impedances derived using different methods that assume different source fields and different geometries (planar or spherical) are often combined to increase the period range available for analysis in order to increase the reliability of the mantle soundings and their interpretation [e.g., *Egbert and Booker*, 1992; *Schultz et al.*, 1993; *Bahr et al.*, 1993; *Semenov and Rodkin*, 1996]. However, the accuracy of such data merges, and a reliable means of achieving their combination, has not been examined and discussed explicitly before; some peculiarities of the joint interpretations of MT and GDS data have been considered after by *Schmucker* [2007].

[4] The mentioned task cannot be realized using the real data over the uncertain deep and subsurface structures in nature. The work presented in this paper attempts to provide an indication of how the different induction methods work on synthetic data prior to their merging and joint interpretation. Another aim of the modeling work is to assess the advantages and shortcomings of some sounding methods to correct sounding curves for the effect of inhomogeneities in the Earth's mantle, including distortion from the near sur-

[1]Geophysics Section, Dublin Institute for Advanced Studies, Dublin, Ireland.
[2]Also at Geophysical Institute, Slovak Academy of Sciences, Bratislava, Slovakia.
[3]Institute of Geophysics, Polish Academy of Sciences, Warsaw, Poland.

0148-0227/10/2009JB006390

face inhomogeneities. The main difficulty, in addition to the selection of the appropriate impedance relationships for the modeling, is the complicated numeric simulation technique required for the generalized HSG method. We believe that this study will help to achieve higher confidence in the results of mantle soundings and to achieve as broad a depth range of investigation of the mantle as possible.

2. Impedance Relationships for Modeling

2.1. Magnetotelluric Approach

[5] The linear MT impedance relationship, considered in the Tikhonov-Cagniard model [*Cagniard*, 1953] for a layered medium, follows also from Rytov's impedance boundary conditions (IBC) for the "weakly" inhomogeneous case [*Rytov*, 1940; *Senior and Volakis*, 1995]. An approximate form of the Rytov's infinite power series with scalar impedance and neglected terms of higher than first order of the spatial derivatives is known as the Leontovich's IBC [*Leontovich*, 1948; *Senior and Volakis*, 1995]. Leontovich's scalar relation, generalized for anisotropic media [*Landau and Lifshic*, 1959; *Senior and Volakis*, 1995], has been applied by Berdichevsky and Cantwell [*Berdichevsky et al.*, 1997] for MT soundings and can be written in the vector form [*Guglielmi*, 2009]:

$$\boldsymbol{E}_\tau \approx \boldsymbol{Z} \cdot (\boldsymbol{H}_\tau \times \boldsymbol{n}). \quad (1)$$

[6] Here $\boldsymbol{Z}$ is the impedance tensor with components $Z_{ij}(\omega, \mathbf{r})$ that depend on the angular frequency ω and the coordinates of the position vector $\mathbf{r}$ at the boundary between conductive (earth) and resistive (air) media; $\boldsymbol{E}_\tau$ and $\boldsymbol{H}_\tau$ are the tangential complex Fourier amplitudes of the electric and magnetic fields, respectively; $\mathbf{n}$ is a unit vector normal to the boundary. The traditional relationship (1) will be used in the modeling of the MT method, though the generalized one on a closed surface has also been derived by *Shuman* [1999, 2003, 2007].

2.2. Magnetovariational Approach

[7] The generalized HSG method also follows from Rytov's IBC in an approximate form under the same condition for the spatial derivatives. The generalized HSG approach was first written out in its explicit form by *Guglielmi and Gokhberg* [1987], which we show in the form

$$-H_z \approx (i\omega\mu_0)^{-1}[Z(div\,\boldsymbol{H}_\tau) + \boldsymbol{H}_\tau \cdot (gradZ)], \quad (2)$$

where $Z(\omega, \mathbf{r})$ is the scalar impedance as defined by *Guglielmi* [2009]; μ_0 is the magnetic permeability of the free space; i is the imaginary unit and H_z is the Fourier amplitude of the magnetic component orthogonal to the Earth's surface. The sign in (2) depends on the chosen reference system. Rytov's IBC, derived for radio wave periods, is valid for cases characterized by large values of the wave number [*Guglielmi*, 1984] or of the refractive index [*Senior and Volakis*, 1995]. These and several other requirements of Rytov's theory are correct for short-period subsurface soundings but they are incorrect for the low frequencies employed for deep induction sounding of the mantle.

[8] A second approach to the generalized HSG sounding method was suggested by *Schmucker* [2003, 2008] and is represented as the combination of the traditional HSG method and the Wise-Parkinson relationship with tippers:

$$B_z = C(\omega) \cdot \{\partial B_{nx}/\partial x + \partial B_{ny}/\partial y\} + z_H B_{nx} + z_D B_{ny} + \delta B_z, \quad (3)$$

where $C(\omega) = Z(\omega)/i\omega\mu_0$ is the scalar C-response, z_H and z_D are the transfer functions (tippers) and δB_z denotes noise. The amplitudes of the observed magnetic field components are subdivided into "normal" (with subscript n) and "anomalous" parts. While the observed vertical component B_z includes both the normal and anomalous parts, the anomalous horizontal field components are neglected in Schmucker's approach, which provides the main distinction from other generalized MV approaches. Examples of applying this approach (3) to real data are also presented by *Schmucker* [2003, 2008].

[9] A third approach to MV soundings is based on the vectoral impedance boundary conditions with two scalar impedances $\zeta(\omega, \mathbf{r})$ and $\xi(\omega, \mathbf{r})$ on a closed surface [*Aboul-Atta and Boerner*, 1975], expanded for the MV method by *Shuman and Kulik* [2002]:

$$i\omega\mu_0 H_\mathrm{r} = \zeta div\boldsymbol{H}_\tau + \boldsymbol{H}_\tau \cdot grad\zeta + \zeta^* div\boldsymbol{H}^*_\tau + \boldsymbol{H}^*_\tau \cdot grad\zeta^*. \quad (4)$$

where H_r is the radial component on the surface of a spherical model, the asterisk indicates the complex conjugate. Shuman's approach (4) coincides with equation (2) if the impedance $\xi^* = 0$ [*Shuman*, 2003, 2007]. In case that $grad\zeta = 0$ for a laterally homogeneous medium and the expression represents the common HSG method:

$$i\omega\mu_0 H_r = \zeta_m\, div\boldsymbol{H}_\tau. \quad (5)$$

[10] Equation (5) will be used in our modeling in sections 3 and 4. Assuming the pure P_1^0 mode for a linearly polarized Dst source at ultralong periods, the expression (5) can be transformed to the relationship of the GDS method [*Olsen*, 1998] written out in geomagnetic spherical coordinates:

$$i\omega\mu_0 H_r^g = \zeta_m^g \cdot 2H_\theta^g/R \cdot tg\theta_\mathrm{o}^g. \quad (6)$$

where $\zeta_m^g(\omega)$ is the impedance of the GDS method, R is the Earth's radius, and θ_o^g is the colatitude of the measurement point. Expression (6) will be used in our modeling.

[11] In practice, all the methods considered above for taking soundings of a medium are applied without a priori knowledge of the medium properties and structure. While theoretically the impedances for all methods should be identical in the case of laterally homogeneous media, in practice it proves almost impossible to locate test sites in which the subsurface is homogeneous. Therefore we use a forward modeling approach to allow us to compare the impedances from each method over known subsurface structures using known fields. We follow the simplest approach for the modeling of the generalized HSG method by using the differential relation (2) as an approximate form of relation (4). We simulate the observed field components on a sphere for a

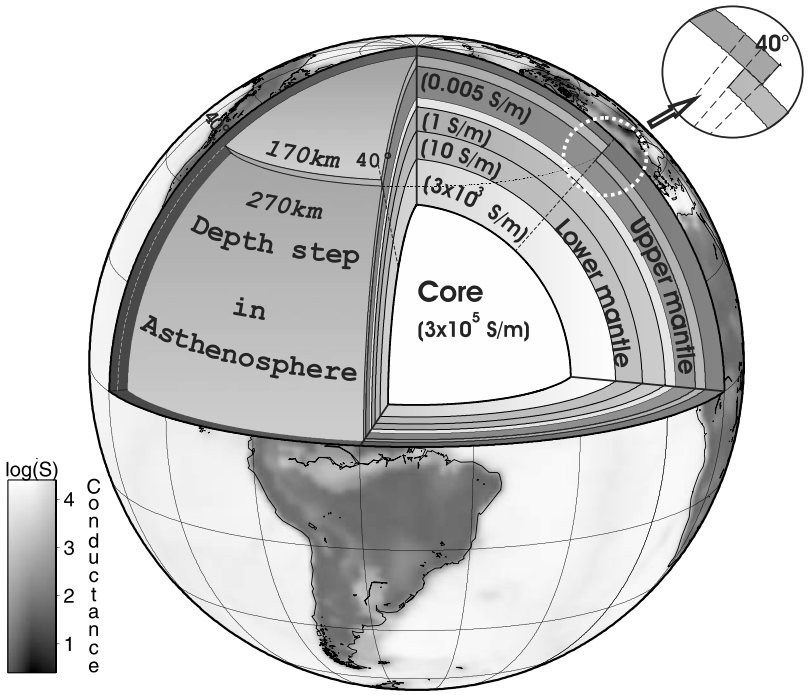

Figure 1. Schematic model of the Earth's conductivity structure assumed in our modeling. The conductances of outer surface shell are used in the final model in Figure 6. In all other models the variable conductance outer shell was replaced with a constant conductance shell (20 S).

number of different structural models without the separation of the fields into "normal" and "anomalous" parts.

3. Method of Numerical Simulation

[12] Forward modeling of the electromagnetic fields excited by ionospheric and magnetospheric sources is carried out on the globe with the alignment of the geographical and geomagnetic reference systems, using the program elaborated by *Kuvshinov et al.* [2005]. The impedances for the MT and "classic" MV methods can be calculated directly from the modeled field components using relations (1), (5), and (6).

[13] The assumed layered Earth structure includes a step in the highly conductive layer of the mantle as shown in Figure 1. The step structure is characterized by a sharp, but not discontinuous, jump in the conductive layer (see the inset in Figure 1), which allows current flow through the structure and therefore maximizes the effects on the fields induced by this mantle inhomogeneity. Spatial distributions of all field components have been computed on the globe at a grid interval of 1° × 1° for a period range from 10 min to 4096 days. Three spherical models were used for testing the methods: 2-D and 3-D spherical models with a homogeneous surface conductance of 20S assumed, and one 3-D spherical model where a realistic surface shell conductance [*Vozar et al.*, 2006] has been taken into consideration (Figure 1).

[14] There are no magnetotelluric plane wave sources for spherical models. But since we work only with impedances, it is sufficient to use horizontal (tangential) source fields that locally depend linearly on the horizontal coordinates [*Berdichevsky and Dmitriev*, 2008]. One can excite the modeled Earth by two polarizations of the source field and thus obtain the tensor of impedances. One requires three polarizations (instead of two in the plane case) in order to avoid the singularities arising globally because of the change of signs of the cos and sin functions. A spherical analog for the "plane wave" source used in the MT method can be approximated by three orthogonal sources of a ring current type. A single ring current is sufficient as a source for modeling in the case of the MV methods based on the expressions mentioned above ((2), (3), (5), and (6)).

[15] The impedances of the generalized HSG method cannot be determined directly from the modeled magnetic field components. Relation (4) with $\xi^* = 0$ has been considered as a differential equation with unknown scalar impedance:

$$(H_\theta/R)\cdot\partial\zeta_m/\partial\theta + \left[H_\varphi/(R\sin\theta)\right]\cdot\partial\zeta_m/\partial\varphi + \zeta_m\left[\partial(H_\theta\cdot\sin\theta)/\partial\theta + \partial H_\varphi/\partial\varphi\right]/(R\cdot\sin\theta) - i\omega\mu_0 H_r = 0. \quad (7)$$

[16] The general solution of equation (7) on the surface of a sphere is obtained for spherical 3-D inhomogeneous structures by using a numerical finite difference method: A simple five-point stencil discretization was applied to derive the central finite difference approximations of derivatives at the spherical grid points. As a result, a system of linear equations (with a small modification of the stencil to an asymmetric one on the grid boundary) has been obtained with the impedances as unknown parameters at all grid points.

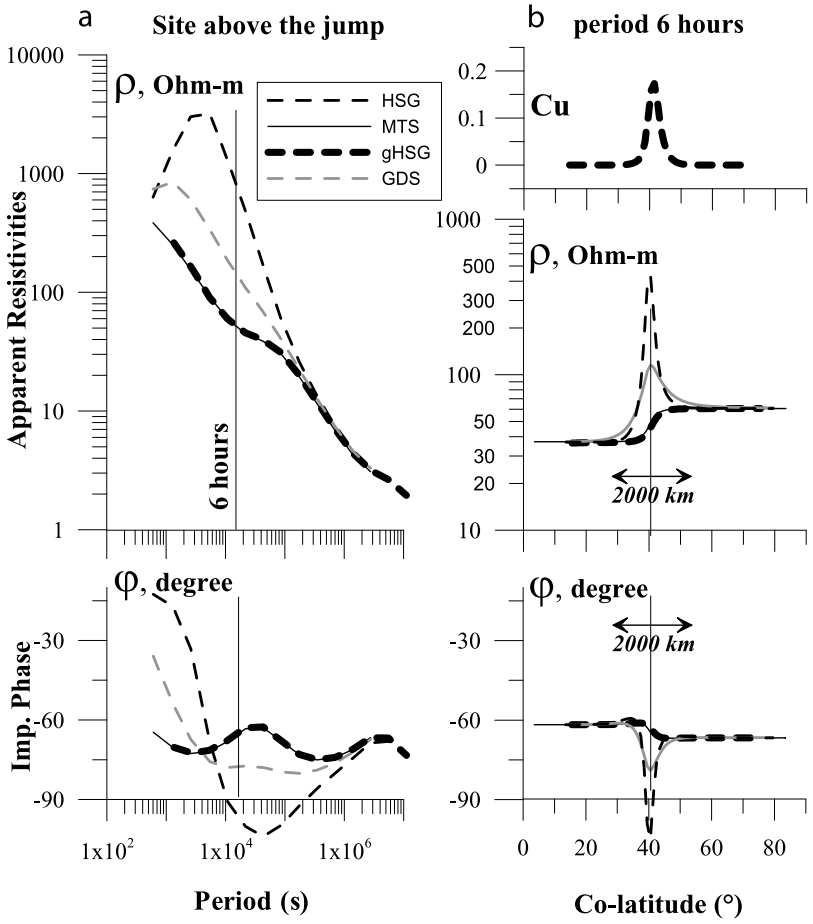

Figure 2. (a) Apparent resistivities (ρ) and impedance phases (φ), directly above the asthenospheric step in the upper mantle, as a function of period. (b) A colatitude profile from the North Pole to the equator, with real induction arrows (*Cu*) for the period 6 h. The responses of the E-polarized MT sounding (MTS) and the HSG, GDS, and generalized HSG (gHSG) methods are shown, as indicated in the legend. Model parameters are described in section 4.

[17] The general equation (7) for the 3-D case was simplified for a 2-D axially symmetric conductivity distribution:

$$(H_\theta/R)\cdot\partial\zeta_m/\partial\theta+[\partial(H_\theta\cdot\sin\theta)/\partial\theta]/(R\cdot\sin\theta)\cdot\zeta_m-i\omega\mu_0H_r=0. \tag{8}$$

[18] The analytical solution for equation (8) on the Earth's surface at a fixed frequency, independent of longitude, can be written in the explicit form [*Semenov et al.*, 2007]:

$$\zeta_m(\theta,\varphi_0,\omega)=e^{-\int_{\theta_0}^{\theta}a(\theta,\varphi_0,\omega)d\theta}\left\{\int_{\theta_0}^{\theta}b(\theta,\varphi_0,\omega)e^{\int_{\theta_0}^{\theta}a(\theta,\varphi_0,\omega)d\theta}d\theta+C_{m0}\right\}, \tag{9}$$

where $C_{m0}=\zeta_m(\theta_0,\varphi_0,\omega)$, $a(\theta,\varphi_0,\omega)=[\partial(H_\theta\cdot\sin\theta)/\partial\theta]/(H_\theta\cdot\sin\theta)$, and $b(\theta,\varphi_0,\omega)=i\omega\mu_0\cdot R\cdot H_r/H_\theta$. The solution (9) establishes the connection between the impedance values at two different points along colatitude profiles (i.e., profiles along a constant line of longitude). A starting (reference) point was chosen at a quasi-homogeneous segment, far from the conductive step in the model, to find impedances and consequently their spatial derivatives along the profile passing over the mantle inhomogeneity (step).

[19] The impedances determined from all sounding methods were converted into the apparent resistivities in the traditional way using the impedance phases. A comparison of the results obtained by the analytical solution (9) with the general numerical solution of equation (7) showed their absolute agreement. The impedance surface distribution found from (7) or (8) was used for the estimation of the induction arrows on the sphere in accordance with the common definition: $\mathbf{C_u}=(Re\{A\};Re\{B\})$, $\mathbf{C_v}=(Im\{A\};Im\{B\})$, where A and B are the gradient tippers:

$$A=[1/(i\omega\mu_0R)]\cdot\partial\zeta_m/\partial\theta$$

$$B=[1/(i\omega\mu_0R\sin\theta)]\cdot\partial\zeta_m/\partial\varphi.$$

[20] In the simplified case of an axially symmetric anomaly such as the step in our model, the gradient tippers

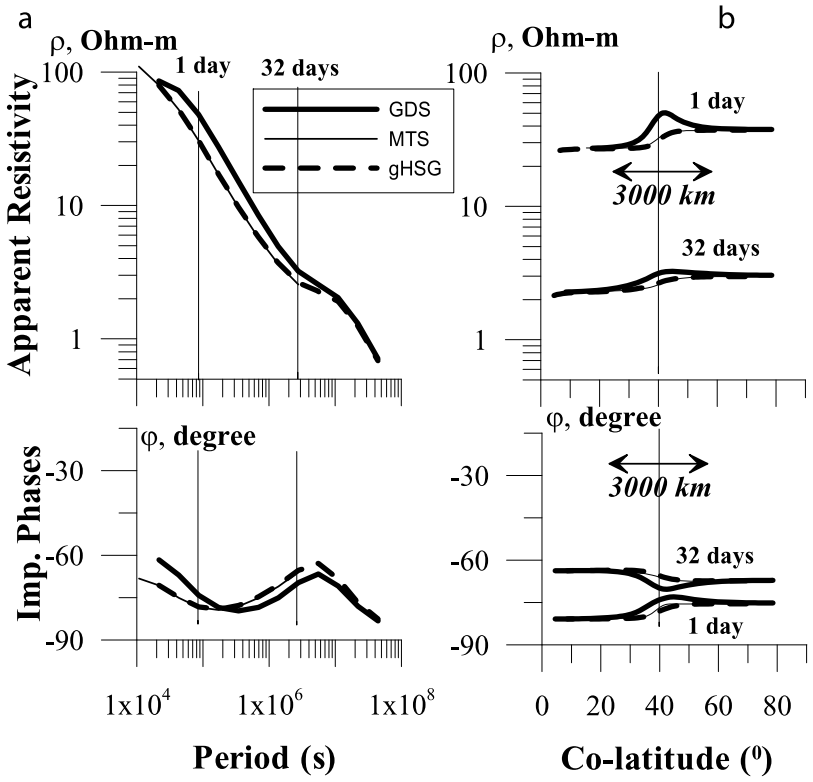

Figure 3. (a) Apparent resistivities (ρ) and impedance phases (φ), directly above the asthenospheric step in the upper mantle, as a function of period. (b) A colatitude profile from the North Pole to the equator, for the period 1 day and 32 days. The responses of the E-polarized MT sounding (MTS) and the GDS and generalized HSG (gHSG) methods are shown, as indicated in the legend. Model parameters are described in section 4.

have only one component A. Then $\mathbf{C_u} = Re\{A\}$ and $\mathbf{C_v} = Im\{A\}$, where $A = H_r - [(\partial(H_\theta \cdot \sin\theta)/\partial\theta)/(\mathbf{R}\cdot\sin\theta \cdot i\omega\mu_0)]\cdot\zeta_m/H_\theta$.

4. Modeling Results

[21] In the first, axially symmetric model of the Earth (Figure 1), the mantle layer (representing the asthenosphere) of 100 km thickness, with conductance of 10 kS, was situated at 170 km below the surface at colatitudes less than 40° measured from the North Pole. In the rest of the model, the layer was situated at the 270 km depth. The source excitations were assumed as discussed in section 3. The MT and generalized HSG responses on the surface directly above the step in the conductive asthenospheric layer were compared with the common HSG and GDS responses. Figure 2 displays the apparent resistivities and impedance phases in the period range from 360 s to 3 months at a chosen point directly above the mantle inhomogeneity (Figure 2a). Figure 2b depicts the real induction arrow, apparent resistivity and impedance phase changes along the colatitude profile from the North Pole to the equator for the period of 6 h. It is clear that the MT and generalized HSG responses are practically the same along the whole profile and for all periods. However, the common HSG and GDS responses are completely different at short periods (up to approximately 10^5 s) and over a distance range of about 20° (2000 km) directly above the step in the model, where the induction arrows are nonzero (see Figure 2b). The common HSG response shows a greater dissimilarity than the GDS case with respect to the MT response.

[22] A second analogous step model was prepared: In this case the conductive midmantle layer has a thickness of 150 km and conductance of 300 kS, and the upper surface of the conductive layer drops from 500 to 650 km depth at the same position as the first model (40° colatitude). The same source excitations have been assumed. The MT and generalized HSG responses are again practically the same for the period range from 0.25 days up to 11 years and along the same profile as for the first model (Figure 3). While the GDS response differs from both the MT and generalized HSG responses at periods up to 10^7 s, the shape of the curves is nevertheless similar, which is a consequence of the step inhomogeneity being located at a greater depth when compared with the first model (Figure 3a). Apparent resistivities and impedance phases obtained from both the MT and generalized HSG methods differ from those for the GDS method over along the distance range of about 30° (3000 km) above the mantle inhomogeneity (Figure 3b).

[23] The third set of models was used to examine the behavior of induction arrows on a spherical Earth. The induction arrows on the Earth's surface presented in Figure 4a are shown directly above steps in a conductive upper mantle layer. The arrows are computed independently for axially symmetric conductivity anomalies situated 1, along the colatitude 40° (latitude 50°); 2, along the colatitude 90° (latitude 0°); and 3, along longitude 0°. The arrows were

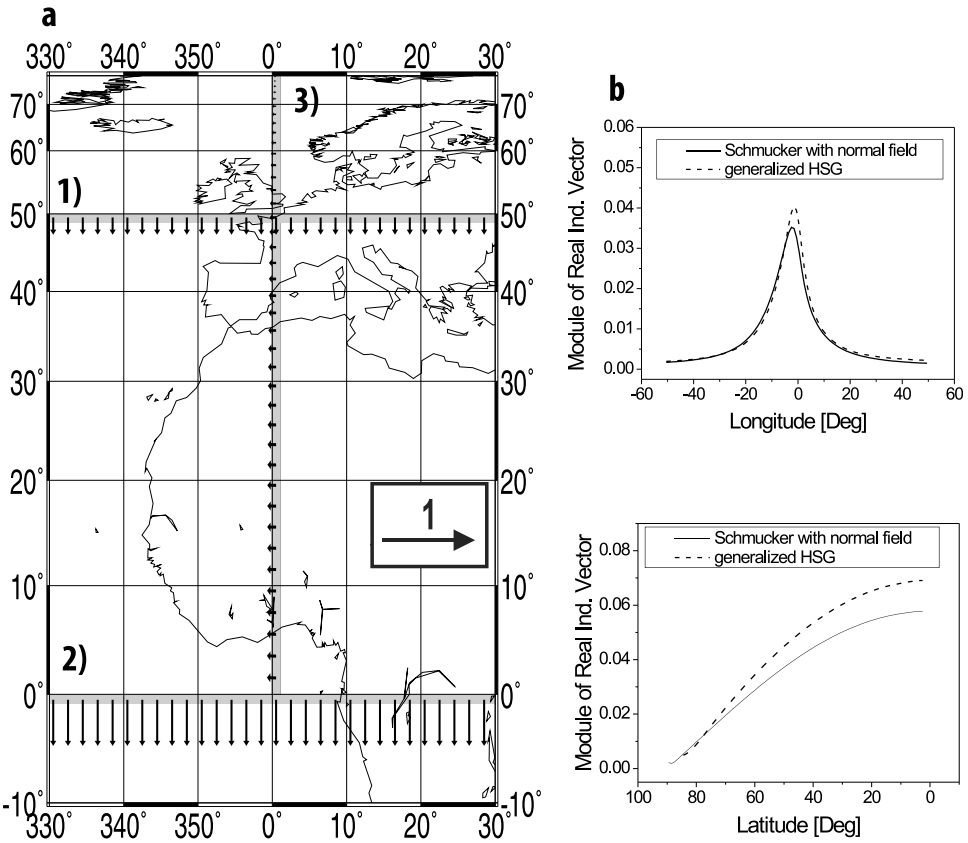

Figure 4. (a) Real induction arrows computed independently for three different models: 1, a mantle step (gray) situated along latitude 50°; 2, a step along the latitude 0°; and 3, a step along longitude 0°. Parameters for the step model are the same as for Figure 2. (b) Profiles of the real induction arrow modulus for model 3 for two methods, generalized HSG (gHSG) and Schmucker's formula with normal field: (top) profile along latitude 55° perpendicularly crossing the anomaly and (bottom) profile along 0° longitude directly above the anomaly.

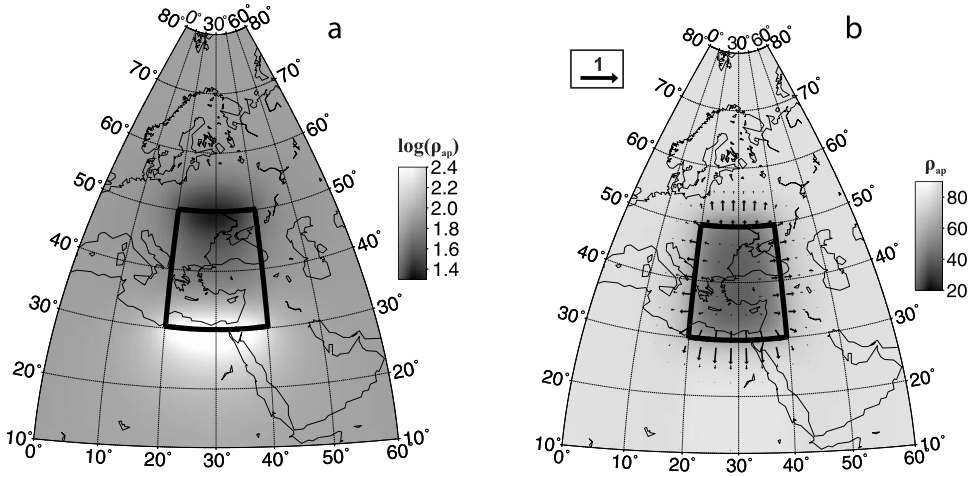

Figure 5. The apparent resistivity anomaly above a 3-D body determined using (a) the GDS method and (b) the generalized HSG method. Source period is 6 h. Real induction arrows are shown in Figure 5b. The anomalous body (thick border) characterized by a resistivity of 10 Ω m is placed within the generalized spherical model of Figure 1 between depths of 170 and 270 km.

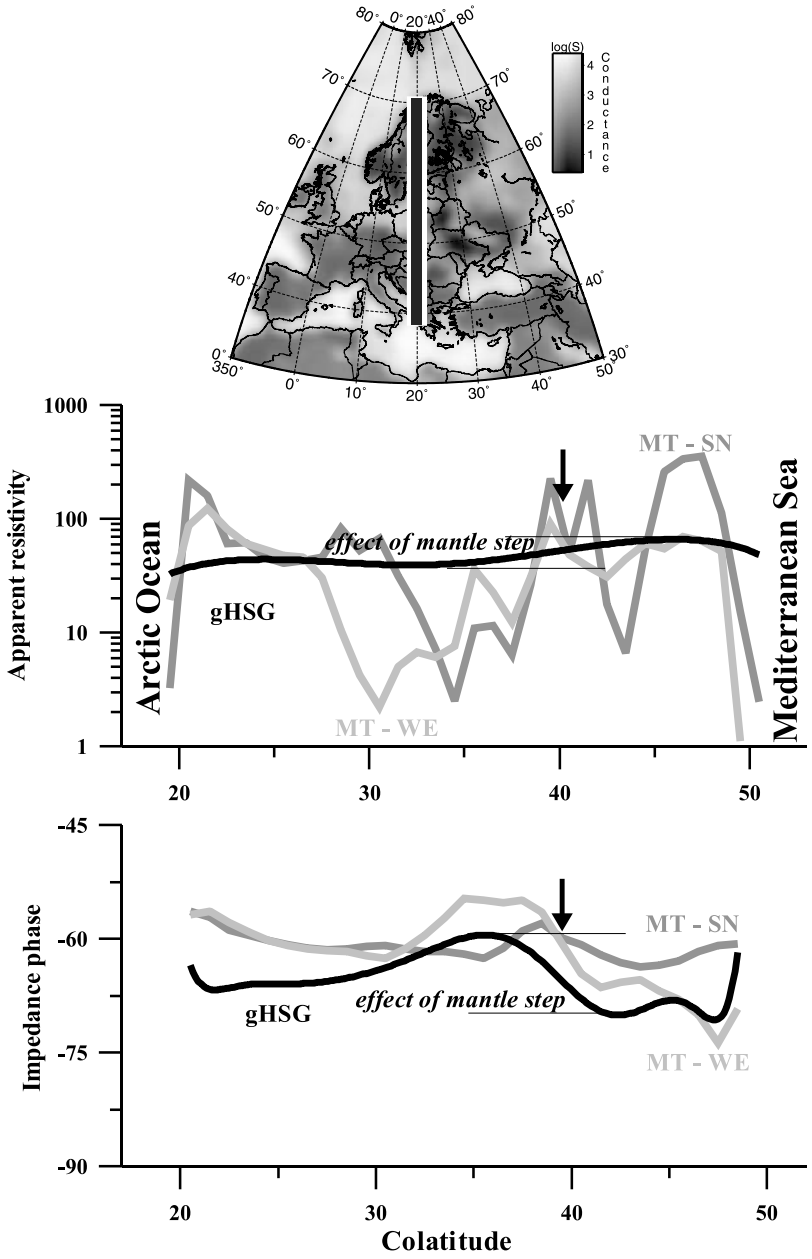

Figure 6. Apparent resistivities and impedance phases modeled by MT soundings for two orthogonal SN and WE directions (gray lines) and by the generalized HSG (gHSG) method (black line). The map at top shows how the profile crosses Europe from the Arctic Ocean to the Mediterranean Sea along a longitude of 20°. The source period is 6 h. Thick arrows indicate the position of the mantle step.

computed numerically using a finite difference method applied to the differential relation (7). Figure 4b shows a comparison of the real induction arrows obtained from the generalized HSG (7) and Schmucker's approach with normal magnetic field on the right side of equation (3). The horizontal normal magnetic field was obtained for a layered radially symmetric Earth with a conductive layer, with no step, anomaly situated at a depth of 170 km. Two profiles of the real induction arrow modulus for model 3 are presented: profile along latitude 55° perpendicularly crossing anomaly (Figure 4b, top); and profile along 0° longitude directly above anomaly (Figure 4b, bottom). The apparent resistivities and phases obtained for Schmucker's approach depend on the chosen normal field.

[24] The results in Figure 4 indicate the quantitative changes in the induction arrows, computed via the gradient tippers on the Earth's surface along latitude, that depend on the position of the inhomogeneity. The moduli of the arrows approach zero near the poles and achieve maximal values near the equator, which is an unusual effect when compared with the common arrows for planar models. Note that the impedance gradients are calculated for the irregular spherical grid instead of the one of uniform distance for the case of the planar Earth model. Both considered approaches (Shuman's and Schmucker's) to the generalized HSG

method show similar results. Although quantitatively the two curves show differences in amplitude, their similar shapes point to the same physical basis.

[25] The next model consists of a 3-D spherical mantle structure in which an anomalous conductive body is placed. The body has a resistivity of 10 Ω m and is located at depths from 170 to 270 km, with horizontal dimensions of 20° × 20° centered on 30° longitude and 50° latitude (Figure 5). Note that anomalous conductive body replaces the asthenospheric step in previous models. The model was considered to be under a source field characterized by pure Dst variation with a period of 6 h. The calculated induced fields on the Earth's surface were used as input data for the numerical solution of relation (7) by the finite difference method. The grid of scalar impedances obtained by the generalized HSG and GDS methods was converted into the apparent resistivities and to gradient tippers which were then used to calculate the induction arrows. The results obtained are presented in Figure 5.

[26] Figure 5a shows that the GDS method is only able to detect the two latitudinal boundaries of the anomaly, where anomalous apparent resistivities are present. In contrast, the generalized HSG method reflects the influence of the whole anomalous body in both the apparent resistivity variation and the orientation of induction arrows.

[27] A final model is considered, consisting of both an asthenospheric step anomaly (see first model Figure 1) and near surface inhomogeneities defined by a surface conductivity map [*Vozar et al.*, 2006]. The generalized HSG and MT responses recalculated into apparent resistivities compared in the principal directions North-south (NS) and east-west (EW) (across or along the step respectively) for the period of 6 h (Figure 6). The profile analyzed is situated along the 20° meridian running from the Arctic Ocean to the Mediterranean Sea (map at top of Figure 6).

[28] It is clear that the anomaly associated with the mantle step, reflected in the MT apparent resistivity distribution, is so weak that it is not visible against the background variations caused by the surface inhomogeneities. Similarly, the anomaly for the same feature obtained by the generalized HSG method is also small (anomaly magnitude is about 20 Ω m) although the method itself is relative insensitivity to the near-surface inhomogeneities. It is worth emphasizing that the generalized HSG and MT impedance phases for the spherical E-polarization (WE direction) have approximately the same shapes directly above the step in the upper mantle layer. As the phase values are disturbed much less by the surface inhomogeneities for both the E-polarization of the MT and generalized HSG methods, it suggests for future work that MT and generalized HSG derived phases could be reliably combined. On the whole, the generalized HSG method, which produces results similar to and compatible with conventional MT impedances, is a promising technique for studies of the Earth's mantle.

5. Conclusions

[29] The principal result of this modeling work is the coincidence of the generalized HSG and MT (without shift effects) responses above the mantle inhomogeneity in the space and frequency domains. It also means that the impedances derived independently from both methods can be combined for joint inversion with confidence, especially in their phases, as has been done in the CEMES project [*Semenov et al.*, 2008]. Our modeling shows the response functions of the common HSG and GDS methods, developed for the sounding of laterally homogeneous Earth structures, can produce responses significantly different from both the generalized HSG and MT responses above mantle inhomogeneities. It means that the traditional 1-D inversion of the common HSG response, and to lesser extent the GDS response, may cause unrealistic inhomogeneous structures.

[30] The problem of merging the MV scalar and MT tensor responses can potentially be solved by the selection of the appropriate directions using mainly for the phase data which are much less sensitive to the galvanic effect. Such choices can be made in several ways in practice [e.g., *Semenov et al.*, 2008]. We note that the advantages of using the phase fit are lost if the real and imaginary part of the C responses or impedances are used instead of their moduli and phases. Note that all of the MV approaches discussed here are also moderately influenced by surface inhomogeneities, manifesting in the magnetic components of the computed field in the period range of several hours [*Everett et al.*, 2003].

[31] The induction arrows calculated from the gradient tippers of the generalized HSG method (as well as using Schmucker's approach) show that the arrows depend on colatitude on the surface of the spherical Earth and represent the real and imaginary parts of the gradient of the scalar magnetovariation C response function. In the case of global soundings, the colatitude trend could therefore play an important role in affecting the reliability of the results.

[32] **Acknowledgments.** The authors appreciate the assistance of Aleksey Kuvshinov, who kindly provided the spherical modeling program. The authors are also grateful to the associate editor Alan Jones, reviewers Ulrich Schmucker and Mark Everett, and many other anonymous reviewers for their valuable remarks. We are thankful to Mark Berdichevsky, Mark Muller, Josef Pek, Vladimir Shuman, and Anatoly Guglielmi for their help and useful discussions. This work has been supported by grant N N307 097437 of the Polish Ministry of Science and Higher Education, by grants VEGA 2/0169/09 and SFI 08/RFP/GEO1693, and by GEODEV-Centre on Geophysical Methods and Observations for Sustainable Development.

References

Aboul-Atta, O. A., and W. M. Boerner (1975), Vectoral impedance identity for the natural dependence of harmonic fields on closed boundaries, *Can. J. Phys.*, *53*(15), 1404–1407.

Bahr, K., N. Olsen, and T. J. Shankland (1993), On the combination of the magnetotelluric and the geomagnetic depth sounding methods for resolving an electrical conductivity increase at 400 km depth, *Geophys. Res. Lett.*, *20*(24), 2937–2940, doi:10.1029/93GL02134.

Banks, R. J. (1969), Geomagnetic variations and the electrical conductivity of the upper mantle, *Geophys. J. R. Astron. Soc.*, *17*, 1–6.

Berdichevsky, M., and V. Dmitriev (2008), *Models and Methods of Magnetotellurics*, Springer, Berlin.

Berdichevsky, M., L. L. Vanyan, and E. B. Fainberg (1969), The frequency soundings of the Earth using spherical analysis results of geomagnetic variations (in Russian), *Geomagn. Aeron., Engl. Transl.*, *9*, 372–374.

Berdichevsky, M., V. Dmitriev, D. B. Novikov, and V. V. Pastucan (1997), *Analysis and Interpretation of the Magnetotelluric Data* (in Russian), p. 6, Dialog, Moscow Univ., Moscow.

Cagniard, L. (1953), Basic theory of magnetotelluric method of geophysical prospecting, *Geophysics*, *18*, 206–210, doi:10.1190/1.1437915.

Egbert, G. D., and J. R. Booker (1992), Very long period magnetotellurics at Tucson observatory: Implications for mantle conductivity, *J. Geophys. Res.*, *97*(B11), 15,099–15,112, doi:10.1029/92JB01251.

Everett, M. E., S. Constable, and C. G. Constable (2003), Effects of near-surface conductance on global satellite induction responses, *Geophys. J. Int.*, *153*, 277–286, doi:10.1046/j.1365-246X.2003.01906.x.

Guglielmi, A. V. (1984), Fore-history of the method of the magnetotelluric sounding (in Russian), *Izvestya, Phys. Solid Earth*, *30*(3), 95–96.

Guglielmi, A. V. (2009), On the fictitious nonlinearity of the surface impedance of the Earth's crust, *JETP Lett.*, *89*(7), 377–380.

Guglielmi, A. V., and M. B. Gokhberg (1987), About magnetotelluric soundings in seismic active zones (in Russian), *Izvestiya, Phys. Earth*, *11*, 122–123.

Hermance, J. F., and W. Wang (1992), "Mode-blind" estimates of deep earth resistivity, *J. Geomagn. Geoelectr.*, *44*, 373–389.

Jones, A. G. (1982), Observations of the electrical asthenosphere beneath Scandinavia, *Tectonophysics*, *90*, 37–55, doi:10.1016/0040-1951(82)90252-9.

Kuckes, A. F. (1973), Relations between electrical conductivity of a mantle and fluctuating magnetic fields, *Geophys. J. R. Astron. Soc.*, *32*, 319–331.

Kuckes, A. F., A. G. Nekut, and B. G. Thompson (1985), A geomagnetic scattering theory for evaluation of earth structure, *Geophys. J.*, *83*(2), 319–330, doi:10.1111/j.1365-246X.1985.tb06489.x.

Kuvshinov, A., H. Utada, D. Avdeev, and T. Koyama (2005), 3-D modeling and analysis of the Dst EM responses in the North Pacific Ocean region, *Geophys. J. Int.*, *160*, 505–526, doi:10.1111/j.1365-246X.2005.02477.x.

Landau, L. D., and E. M. Lifshic (1959), *Electrodynamics of Continuums* (in Russian), Phys. Math. Literature, Moscow.

Leontovich, M. A. (1948), Approximate boundary conditions for the electromagnetic field on the surface of a good conductor, in *Investigations on Radiowave Propagation* (in Russian), pp. 5–12, Akad. Nauk. SSSR, Moscow.

Lilley, F. E. M., D. V. Woods, and M. N. Sloane (1981), Electrical conductivity from Australian magnetometer arrays using spatial gradient data, *Phys. Earth Planet. Inter.*, *25*, 202–209, doi:10.1016/0031-9201(81)90062-5.

Logvinov, I. M. (2002), Applying of the horizontal spatial gradient method for the deep conductivity estimations in the Ukraine, *Acta Geophys. Pol.*, *50*(4), 567–574.

Olsen, N. (1998), The electrical conductivity of the mantle beneath Europe derived from C-responses from 3 to 720 hr, *Geophys. J. Int.*, *133*, 298–308, doi:10.1046/j.1365-246X.1998.00503.x.

Roberts, R. G. (1984), The long period electromagnetic response of the Earth, *Geophys. J. R. Astron. Soc.*, *78*(2), 547–572.

Rytov, S. M. (1940), Estimation of the skin-effect by the perturbation method (in Russian), *J. Exp. Theor. Phys.*, *10*(2), 180–189.

Schmucker, U. (1970), Anomalies of geomagnetic variations in southwestern United States, *Bull. Scripps Inst. Oceanogr. Univ. Calif.*, *13*, 233–256.

Schmucker, U. (2003), Horizontal spatial gradient sounding and geomagnetic depth sounding in the period range of daily variation, in *Protokoll über das Kolloquium elektromagnetische Tiefenforschung*, edited by A. Hördt and J. Stoll, pp. 228–237, Bibliothek des Wiss. Albert Einstein, Potsdam, Germany.

Schmucker, U. (2007), Integral equations for the interpretation of MT and GDS results, paper presented at 22 Kolloquium Elektromagnetische Tiefenforschung, Decin, Czech Republic, 1–5 Oct.

Schmucker, U. (2008), Comparative induction studies with geomagnetic observatory data in three epoch, paper presented at 19th Electromagnetic Induction in the Earth Workshop, Beijing, China, October 23–29.

Schultz, A., and J. C. Larsen (1987), On the electrical conductivity of the mid-mantle: I. Calculation of equivalent scalar magnetotelluric response function, *Geophys. J. R. Astron. Soc.*, *88*, 733–761.

Schultz, A., R. D. Kurtz, A. D. Chave, and A. G. Jones (1993), Conductivity discontinuities in the upper mantle beneath a stable craton, *Geophys. Res. Lett.*, *20*(24), 2941–2944.

Semenov, V. Y., and M. V. Rodkin (1996), Conductivity structure of the upper mantle in an active subduction zone, *J. Geodyn.*, *21*(4), 355–364, doi:10.1016/0264-3707(95)00038-0.

Semenov, V. Y., J. Vozar, and V. Shuman (2007), A new approach to gradient geomagnetic sounding, *Izvestiya, Phys. Solid Earth*, *43*(7), 592–596, doi:10.1134/S1069351307070087.

Semenov, V. Y., J. Pek, A. Ádám, W. Jóźwiak, B. Ladanyvskyy, I. M. Logvinov, P. Pushkarev, and J. Vozar (2008), Electrical structure of the upper mantle beneath Central Europe: Results of the CEMES project, *Acta Geophys.*, *56*(4), 957–981, doi:10.2478/s11600-008-0058-2.

Senior, T. B. A., and J. L. Volakis (1995), *Approximate Boundary Conditions in Electromagnetics*, 353 pp., IEE Press, London.

Shuman, V. N. (1999), Exact scalar impedance boundary conditions in geoelectromagnetic investigation, paper presented at the Second International Symposium on Three Dimensional Electromagnetics, Salt Lake City, Utah, 24–26 Oct.

Shuman, V. N. (2003), The general theory of geoelectromagnetic sounding systems accounting the electrodynamics of spherical sources, paper presented at the 3D EM-3 Workshop, Adelaide, Australia, 20–21 Feb.

Shuman, V. N. (2007), Imaginary surface vectors in multidimensional inverse problems of geoelectrics, *Izvestiya, Phys. Solid Earth*, *43*(3), 592–596.

Shuman, V. N., and S. Kulik (2002), The fundamental relations of impedance type in general theories of the electromagnetic induction studies, *Acta Geophys. Pol.*, *50*(4), 607–618.

Vozar, J., V. Y. Semenov, A. Kuvshinov, and C. Manoj (2006), A new subsurface map of the Earth conductance, *Eos Trans. AGU*, *87*(33), 326, 331.

V. Y. Semenov, Institute of Geophysics, Polish Academy of Sciences, Ksiecia Janusza 64, 01-452 Warsaw, Poland.

J. Vozar, Geophysics Section, Dublin Institute for Advanced Studies, Merrion Square 5, Dublin 2, Ireland. (vozar@cp.dias.ie)